Recombinant Human Thyroid-Stimulating Hormone Versus Thyroid Hormone Withdrawal in ^{124}I PET/CT–Based Dosimetry for ^{131}I Therapy of Metastatic Differentiated Thyroid Cancer

Donika Plyku[1], Robert F. Hobbs[1,2], Kevin Huang[1], Frank Atkins[3], Carlos Garcia[3], George Sgouros[1,2], and Douglas Van Nostrand[3]

[1]Department of Radiology, Johns Hopkins University, School of Medicine, Baltimore, Maryland; [2]Department of Radiation Oncology, Johns Hopkins University, School of Medicine, Baltimore Maryland; and [3]Medstar Health Research Institute and Division of Nuclear Medicine, MedStar Washington Hospital Center, Washington, District of Columbia

Patients with metastatic differentiated thyroid cancer (DTC) may be prepared using either thyroid-stimulating hormone withdrawal (THW) or recombinant human thyroid-stimulating hormone (rhTSH) injections before ^{131}I administration for treatment. The objective of this study was to compare the absorbed dose to the critical organs and tumors determined by ^{124}I PET/CT–based dosimetry for ^{131}I therapy of metastatic DTC when the same patient was prepared with and imaged after both THW and rhTSH injections. **Methods:** Four DTC patients at MedStar Washington Hospital Center were first prepared using the rhTSH method and imaged by ^{124}I PET/CT at 2, 24, 48, 72, and 96 h after administration of approximately 30–63 MBq of ^{124}I. After 5–8 wk, the same patients were prepared using the THW method and imaged as before. The ^{124}I PET/CT images acquired as part of a prospective study were used to perform retrospective dosimetric calculations for ^{131}I therapy for the normal organs with the dosimetry package 3D-RD. The absorbed doses from ^{131}I for the lungs, liver, heart, kidneys, and bone marrow were obtained for each study (rhTSH and THW). Twenty-two lesions in 3 patients were identified. The contours were drawn on each PET image of each study. Time-integrated activity coefficients were calculated and used as input in OLINDA/EXM sphere dose calculator to obtain the absorbed dose to tumors. **Results:** The THW-to-rhTSH organ absorbed dose ratio averaged over 5 organs for the first 3 patients was 1.5, 2.5, and 0.64, respectively, and averaged over 3 organs for the fourth patient was 1.1. The absorbed dose per unit administered activity to the bone marrow was 0.13, 0.086, 0.33, and 0.068 mGy/MBq after rhTSH and 0.11, 0.14, 0.22, and 0.080 mGy/MBq after THW for each patient, respectively. With the exception of 3 lesions of 1 patient, the absorbed dose per unit administered activity of ^{131}I was higher in the THW study than in the rhTSH study. The ratio of the average tumor absorbed dose after stimulation by THW compared with stimulation by rhTSH injections was 3.9, 27, and 1.4 for patient 1, patient 2, and patient 3, respectively. The ratio of mean tumor to bone marrow absorbed dose per unit administered activity of ^{131}I, after THW and rhTSH, was 232 and 62 (patient 1), 12 and 0.78 (patient 2), and 22 and 11 (patient 3), respectively. **Conclusion:** The results suggest a high patient variability in the overall absorbed dose to the normal organs per MBq of ^{131}I administered, between the 2 TSH stimulation methods. The tumor–to–dose-limiting-organ (bone marrow) absorbed dose ratio, that is, the therapeutic index, was higher in the THW-aided than rhTSH-aided administrations. Additional comparison for tumor and normal organ absorbed dose in patients prepared using both methods is needed before definitive conclusions may be drawn regarding rhTSH versus THW patient preparation methods for ^{131}I therapy of metastatic DTC.

Key Words: dosimetry; imaging; differentiated thyroid cancer; radionuclide therapy; radiopharmaceuticals

J Nucl Med 2017; 58:1146–1154
DOI: 10.2967/jnumed.116.179366

Sodium iodine labeled with ^{131}I (^{131}I-NaI) is used for the treatment of distant metastases of differentiated thyroid cancer (DTC). To enhance uptake of ^{131}I by the metastatic thyroid tissue, patients are prepared for therapy by either thyroid hormone withdrawal (THW) or injection of recombinant human thyroid-stimulating hormone (rhTSH). Although rhTSH injections have been approved by the Food and Drug Administration for the preparation of patients for diagnostic radioiodine scans as well as for ^{131}I remnant ablation of thyroid tissue, the use of rhTSH injection is not approved by the Food and Drug Administration or the European Medicines Agency for preparation of patients for ^{131}I treatment of distant metastases of DTC. For the absorbed dose to tumors, only a few reports have been published (*1–4*) comparing methods of preparation using either THW or rhTSH injections, and further study is warranted. For the absorbed dose to nontumor tissues, more reports have been published. These publications typically evaluated whole-body or bone marrow dosimetry using ^{131}I or ^{123}I; used dosimetry calculation methods that were not specifically developed for radiopharmaceutical therapy, which are not as quantitative as ^{124}I PET/CT–based methods, and were not necessarily performed in patients with metastatic disease; or did not compare THW versus rhTSH injections in the same patient (*3–8*). The objective of this study was 3-fold: to calculate the absorbed dose to bone marrow and multiple other critical organs (e.g., lung, liver, heart, and kidneys) using ^{124}I PET/CT and dosimetry software that specifically accounts for patient anatomy and activity distribution (e.g., 3D-RD) in patients with metastatic DTC; to calculate the absorbed dose to tumors and the tumor–to–dose-limiting

Received Jun. 6, 2016; revision accepted Dec. 8, 2016.
For correspondence or reprints contact: Douglas Van Nostrand, Nuclear Medicine Research, MedStar Health Research Institute and Washington Hospital Center, Georgetown University School of Medicine, Suite GA60F, 110 Irving St., N.W. Washington, DC 20010.
E-mail: douglas.van.nostrand@medstar.net
Published online Jan. 19, 2017.

TABLE 1
Patient Demographics

Characteristic	Patient 1	Patient 2	Patient 3	Patient 4
Age (y)	47	30	63	51
Sex	M	M	M	M
Thyroglobulin level (ng/mL)	170*; 324†	NA*; 1,527†	3,735*; 2,480†	86*; 58†
TSH level (μIU/mL)	98*; 82.9†	139*; 142†	89*; 124†	64*; 72†
Urine iodine level (μg/L)	182‡; 85†	75‡; 630†	99‡; NA†	28‡; 21†
Thyroxine dose before and during rhTSH stimulation (μg)	125	125	139	200

*Under rhTSH.
†Under THW.
‡Before rhTSH.
NA = not applicable.

organ absorbed dose ratio for both studies (rhTSH and THW); and to compare the absorbed doses to those critical organs and tumors after preparation with THW versus rhTSH, with the patient being his own control.

MATERIALS AND METHODS

Four male patients at MedStar Washington Hospital Center, diagnosed with metastatic DTC, referred for ^{131}I dosimetry were included in this study. The study was approved by the MedStar Institutional Review Board, and all patients signed a written informed consent form. Each patient was placed on a low-iodine diet for 14 d before beginning dosimetry and continuing until the day after completion of the first ^{124}I scan. Patients were prepared with intramuscular injections of rhTSH (0.9 mg) on 2 consecutive days. At approximately 24 h after the second rhTSH injection, 30–63 MBq (0.8–1.7 mCi) of ^{124}I were administered orally. PET/CT imaging was performed at 2, 24, 48, 72, and 96 h after ^{124}I administration. Patients were imaged on a Philips Gemini (time-of-flight) PET/CT camera. The whole-body scans were acquired using 16 bed positions. The field of view for each bed position was 18 cm in length. Depending on the acquisition time after administration, imaging duration was 2 or 4 min/bed position.

Approximately 5–8 wk later, the same patient was prepared using THW. The patient discontinued his thyroxine and began liothyronine sodium (Cytomel; Pfizer) (25 μg 2–3 times a day for 21 d). Liothyronine sodium was discontinued starting 14 d before the second oral ^{124}I administration through the diagnostic imaging period and until the day after ^{131}I therapy. The patient was also placed on a low-iodine diet 14 d before beginning the second round of imaging for dosimetry; the low-iodine diet was continued until the day after ^{131}I therapy. Serial ^{124}I PET/CT scans were again collected as described above.

Patients Demographics

The 4 patients are notated as patient 1, patient 2, patient 3, and patient 4. Demographics and relevant clinical parameters are tabulated in Table 1. The ^{124}I administered activity for each study and the administered activity before ^{131}I therapy for each patient are given in Table 2.

Activity Quantification

The sensitivity of the Philips Gemini time-of-flight camera was measured by scanning an ^{124}I standard of a known ^{124}I activity and was determined to be 296 cps/MBq. The ^{124}I sample was placed in a vial, and the activity was measured using a dose calibrator. The vial was positioned at the center of the field of view of the PET/CT camera and imaged using a single-bed scan.

Overview of Dose Calculation Approach

Normal tissue absorbed doses were obtained using the previously developed software package 3D-RD. Given the overall comparative nature of the study, many of the key features of 3D-RD, namely radiobiologic modeling and voxelized dosimetry, were not used; nevertheless, the use of personal anatomy of each patient justifies using such personalized software. Likewise, the tumor absorbed dose calculations were performed using standard methods rather than a voxelized approach and radiobiologic modeling.

Dosimetry Calculations for Normal Organs

The activity for ^{124}I was calculated for each organ volume of interest (VOI) and divided by the administered activity of ^{124}I to obtain the percentage injected activity (%IA). The %IA, divided by the organ volume in cm^3, yielded the percentage injected activity concentration (%IA/cm^3) for each organ VOI. The time-integrated activity coefficient for ^{124}I was obtained by dividing the time-integrated activity or area under the curve by the ^{124}I injected activity values given in Table 2.

The ^{124}I PET/CT images were used as input to 3D-RD, the personalized dosimetry software package (*9–12*), to obtain absorbed dose to normal organs for ^{131}I therapy. 3D-RD is a patient-specific, 3-dimensional image-based dosimetry package that involves use of patient's own anatomy and spatial distributions of radioactivity over time to perform absorbed dose calculations.

The PET activity data were corrected for the difference in physical decay between ^{124}I and ^{131}I according to Equation 1:

$$A_{I^{131}}(t) = A_{I^{124}}(t) \times e^{(\lambda_{I124} - \lambda_{I131})t}, \qquad \text{Eq. 1}$$

where $A(t)$ represents activity at a measured time point t after ^{124}I administration.

TABLE 2
^{124}I and ^{131}I Administered Activities

	^{124}I activity (MBq)		^{131}I activity	
Patient no.	rhTSH	THW	mCi	MBq
1	30	29	319	11,803
2	61	65	398	14,726
3	36	33	198	7,326
4	37	33	326	12,062

The ^{131}I absorbed dose to the lungs, heart, liver, kidneys, and bone marrow was calculated using 3D-RD. The absorbed dose to salivary glands, also an organ of concern in ^{131}I therapy, was not evaluated because the pharmacokinetics of radioiodine in the salivary glands are susceptible to a large number of physiologic processes (e.g., eating, chewing, visual stimuli, spontaneous salivation) such as the pharmacokinetics are minute by minute and cannot be reliably evaluated with the available time–activity data points of days (*13*). The standard 3D-RD workflow is a series of steps of image processing, Monte Carlo simulation, and data analysis, and more detailed descriptions are given by Sgouros et al. (*9*), Prideaux et al. (*10*), and Hobbs et al. (*14*). Herein, we briefly outline each step of the 3D-RD calculation.

Image Registration and VOI Determination

First, all the serial PET/CT images for both THW and rhTSH injection studies were registered across time to the first-time-point CT image of the study prepared with rhTSH injections, using a nonrigid or deformable registration algorithm with the imaging software Velocity (Varian Medical Systems Inc.). For each patient, VOIs encompassing the heart, lungs, liver, kidneys, and bone marrow were drawn manually using either HERMES imaging software (HERMES Medical Solutions) or Velocity on the patients' CT images. VOIs covering the thoracic and lumbar vertebrae (between T9 and L4, depending on the patient) were drawn to estimate the absorbed dose to bone marrow. Figure 1 shows superimposed CT and PET images and example organ VOIs. The metastases for patients 1 and 2 were located in the lungs. To separate the dose to the lungs from the absorbed dose to tumors, the tumor volumes were excluded from the lungs' VOIs. The heart wall could not be distinguished on CT, and therefore the dose calculation represents dose averaged over heart wall and contents. A streak artifact in the CT image of patient 4 affected the attenuation correction of the serial PET images for this patient and specifically the bed position covering part of the liver and the kidneys. For this reason, these 2 organs were not included in the dose calculations for patient 4.

Image Processing and Monte Carlo Simulation

The registered CT and PET images were used in 3D-RD to generate patient-specific anatomy and patient- and study-specific activity images. The attenuation image derived from CT was used to define the corresponding spatial tissue density (density map) and composition (materials map) distributions. Dose rate images were obtained at each time point by Monte Carlo simulation with the energy spectrum of ^{131}I emissions, obtained from the MIRD radionuclide data and decay scheme database (*15*).

VOI-Based Analysis

The energy deposition from Monte Carlo simulation was scored for each time point in each VOI and divided by the mass of the VOI, obtained from CT, to calculate the dose rate. The dose rate values for almost all normal organ VOIs exhibited a single-phase clearance over the measured time points and were fit using a monoexponential function. The one exception was for the lung VOI of patient 2 THW study, which exhibited a period of uptake and was fit using a hybrid (trapezoidal–exponential) fit consisting of linear fits between the first 2 time points and an exponential tail obtained by fitting to the final 3 time points. The period of uptake observed in the lungs is consistent with the presence of diffuse lung metastases. The integration of the curve was calculated in each case to obtain the absorbed dose.

Bone Marrow Dosimetry

VOIs covering the thoracic and lumbar vertebrae (between T9 and L4, depending on the patient) were manually drawn on the CT images for bone marrow dosimetry. The volumes of bone marrow VOIs were 120, 134, 94, and 53 mL for patient 1, patient 2, patient 3, and patient 4, respectively. No corrections were made for partial-volume effects.

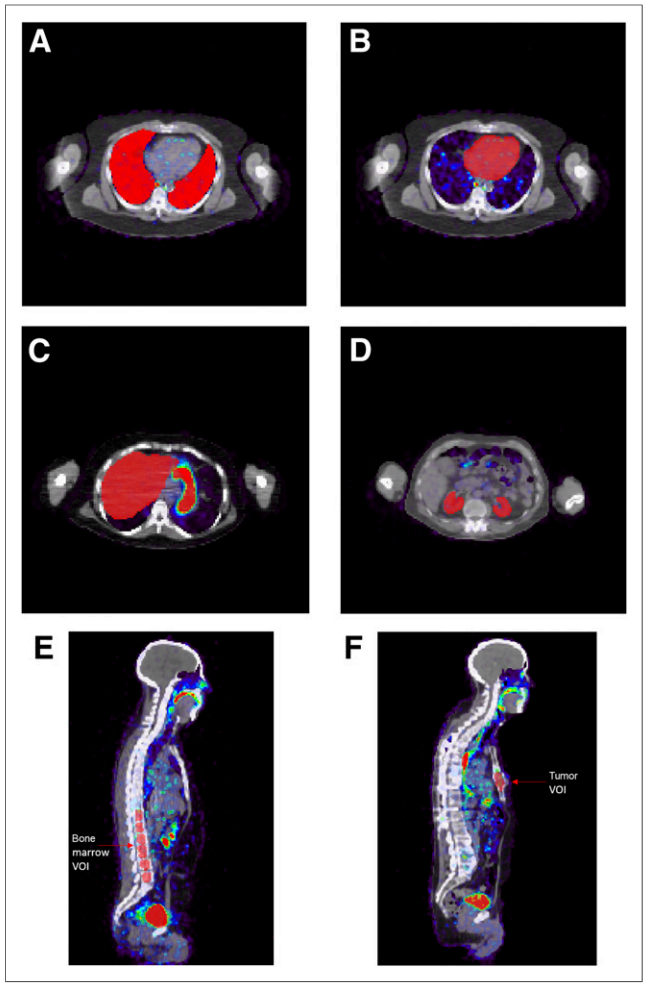

FIGURE 1. Transverse and sagittal views of patients' CT and PET images (superimposed) and drawn VOIs covering lungs (A), heart (B), liver (C), kidneys (D), bone marrow (E), and tumor (F).

The bone marrow activity was obtained from the serial PET images, and marrow dose calculations were performed by following the 3-dimensional imaging–based method described in Woliner-van der Weg et al. (*16*), with the exception that CT-drawn VOIs instead of functional image–based VOIs were used here. No further assumptions or corrections were made in the bone marrow dose calculations.

Dosimetry Calculations for Tumors

Detailed tumor dosimetry calculations were performed according to the MIRD formalism given in pamphlet 21 (*17*). Twenty-two tumors were identified: 9, 2, and 11 tumors in 3 patients. Initially, tumor contours were drawn on the CT image using the imaging software HERMES (HERMES Medical Solutions) with the guidance of a nuclear medicine physician. The volumes of the tumors were measured from the drawn anatomic structures and ranged from 0.38 to 47 cm^3. Figure 1F shows a representative tumor VOI.

To account for the partial-volume effect, the tumor activity uptake was measured by delineating individual contours for each-time-point PET image of the 2 studies, rhTSH and THW, of each patient. A total of 220 contours were drawn for the 3 patients with metastases (patients 1–3). Figure 2 depicts the method used to obtain the tumor activity in the region of interest. The tumor contours were drawn with the imaging software Velocity using a minimum threshold of the maximum PET value for each image and tumor. The volume of the

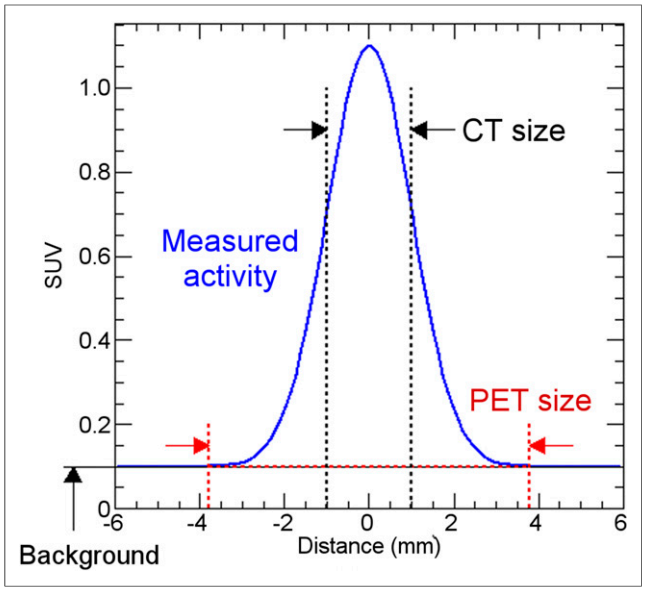

FIGURE 2. Activity measurement method in tumors.

drawn tumor contour on each PET image varied from the true volume (the volume identified from the anatomic contour drawn on the CT image; CT size in Fig. 2). The background activity concentration was also measured by drawing contours on the PET scan at specific locations in the patient's body, that is, bone, bone marrow, and lungs, according to the tumor locations. Background activity was calculated as the product of the measured background activity concentration (counts/cm^3) and the PET-based tumor contour volume (cm^3) (PET size in Fig. 2) and subsequently subtracted from the measured tumor activity (counts). The product of the background activity concentration with the true tumor volume was then added back into the measured tumor activity (Fig. 2).

Measured tumor activity at each time point was used to generate time–activity curves for each tumor and study. Time–activity curves were then integrated using a piecewise hybrid trapezoidal fit in the uptake phase of the tumor, followed by a single-exponential fit in the clearance phase, that is, from the last 3 time points. Time-integrated activity coefficients (previously known as residence times) were calculated for each tumor by dividing the time-integrated activity by the administered activity for ^{131}I, given in Table 2. The time-integrated activity coefficients were used as input in the expression used to calculate the absorbed dose according to the MIRD schema (*17*). A power-law function was fit to calculate the S value ($r_T \leftarrow r_S$) (the radionuclide-specific quantity representing the mean absorbed dose rate to target tissue r_T at time t, after administration per unit activity present in source tissue r_S) for intermediate tumor mass values, based on the OLINDA/EXM (*18*) module for estimation of spheric tumor self-dose according to Equation 2:

$$S = a \times m^b, \qquad \text{Eq. 2}$$

where S is the S value in mGy/MBq-hr, m is the tumor mass in g, and a = 108 mGy/MBq-hr-g and b = −0.97 are parameters specific to ^{131}I.

To account for the cross-dose component from ^{131}I photons in the dose calculation to tumors, the whole-body to whole-body photon dose contribution from ^{131}I was calculated in OLINDA using the measured whole-body time-integrated activity over the measured time points for each study. This contribution was added to the calculated spheric tumor self-dose to obtain the total absorbed dose to tumors from ^{131}I.

To compare aggregate tumor kinetics relative to bone marrow kinetics for each patient, we summed the activity in all tumors at each time point and divided by the total tumor mass. This was used to plot an aggregate tumor activity versus time curve that may be compared with the bone marrow time–activity curve under each preparation method.

RESULTS

Figure 3 shows the %IA/cm^3 as a function of time after ^{124}I administration and the clearance half-lives for 5 organs and each study. The rhTSH clearance half-life was longer than that of THW for bone marrow for patients 1 and 4 and all studied organs for patient 3. The rhTSH clearance half-life was faster than that of

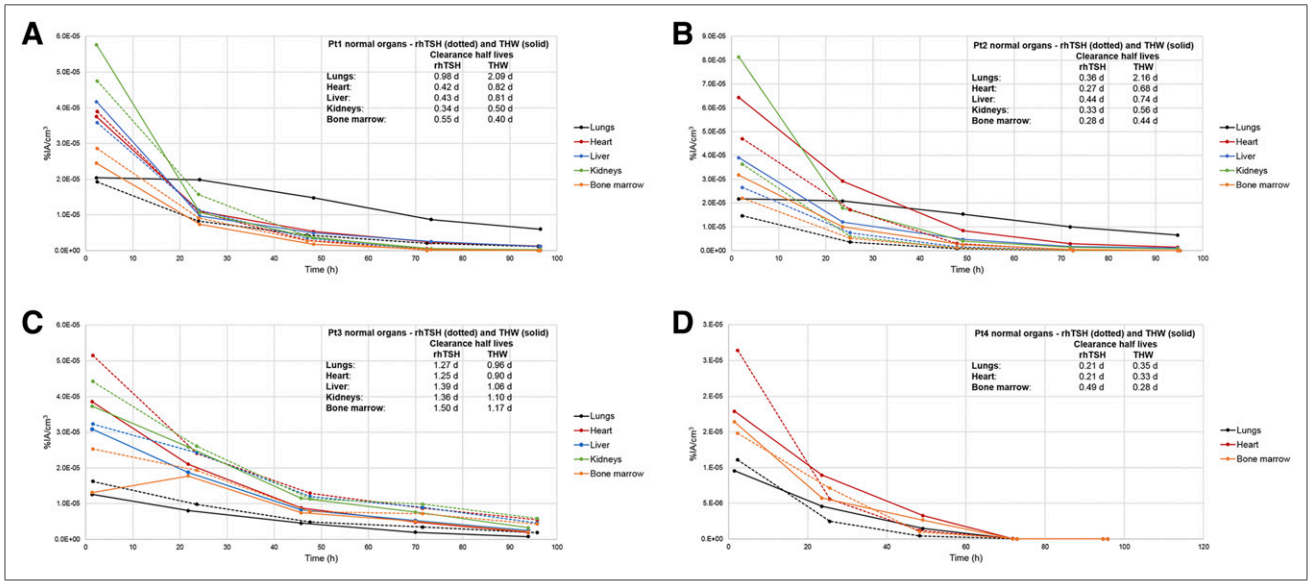

FIGURE 3. Normal organ %IA/cm^3 vs. time (hr) after injection of ^{124}I for rhTSH and THW for patient 1 (A), patient 2 (B), patient 3 (C), and patient 4 (D). Pt = patient.

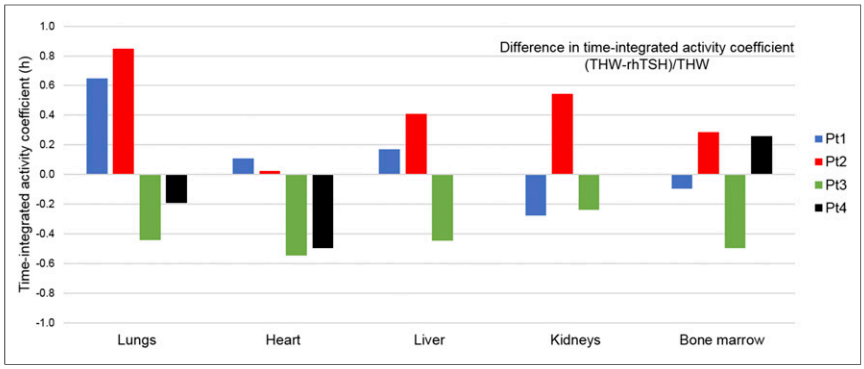

FIGURE 4. Difference in time-integrated activity coefficient (THW − rhTSH)/THW.

THW for the rest of the studied organs. The following organs exhibited a higher initial uptake in the rhTSH study than in the THW study: the heart and bone marrow for patient 1, all the studied organs for patient 3, and the lungs and heart for patient 4. The initial uptake for the rest of the organs was lower in the rhTSH study than in the THW study.

The difference in the obtained time-integrated activity coefficients between THW and rhTSH divided by the time-integrated activity coefficient of the THW study is shown in Figure 4. The time-integrated activity coefficient for the kidneys and bone marrow of patient 1, all studied organs of patient 3, and lungs and heart of patient 4 was higher in the rhTSH study than in the THW study. The time-integrated activity coefficient was lower in the rhTSH than in the THW for the rest of the organs.

The normal organ absorbed dose results are summarized in Table 3. The absorbed dose per unit administered activity is lower in the THW study than in the rhTSH study for the kidneys and bone marrow of patient 1 and heart of patient 4, and higher for the rest of the organs for patient 1 and patient 4. For patient 2, the absorbed dose per unit administered activity is higher in THW than in rhTSH for all studied organs. For patient 3, the absorbed dose per unit administered activity is lower in THW than in rhTSH for all studied organs. The observations on the difference in time-integrated activity coefficients between rhTSH and THW translate to the difference in the absorbed dose results between rhTSH and THW for patients 1–3.

The THW-to-rhTSH absorbed dose per unit administered activity of ^{131}I ratio, averaged over 5 organs (lungs, heart, liver, kidneys, and bone marrow) for patient 1, patient 2, and patient 3, was 1.5, 2.5, and 0.64, respectively. The THW-to-rhTSH absorbed dose ratio averaged over 3 organs (lungs, heart, and bone marrow) was 1.1 for patient 4. The bone marrow absorbed dose per unit administered activity was 0.13, 0.086, 0.33, and 0.068 mGy/MBq after rhTSH and 0.11, 0.14, 0.22, and 0.080 mGy/MBq after THW, for patient 1, patient 2, patient 3, and patient 4, respectively.

With the exception of 3 lesions (with volumes 3.8, 4.3, and 12 cm^3), the absorbed dose per unit administered activity of ^{131}I was higher in the THW study than in the rhTSH study. Table 4 lists the total absorbed dose per unit administered activity for

TABLE 3
Absorbed Dose per Unit Administered Activity of ^{131}I for Each Study (rhTSH and THW) and Ratio in Absorbed Dose per Unit Administered Activity (THW/rhTSH)

Patient	Organ VOI				
	Lungs	Heart	Liver	Kidneys	Bone marrow
1					
Absorbed dose per unit administered activity for rhTSH (mGy/MBq)	0.21	0.15	0.15	0.19	0.13
Absorbed dose per unit administered activity for THW (mGy/MBq)	0.58	0.21	0.19	0.17	0.11
THW/rhTSH ratio	2.8	1.4	1.3	0.9	0.85
2					
Absorbed dose per unit administered activity for rhTSH (mGy/MBq)	0.11	0.27	0.11	0.11	0.086
Absorbed dose per unit administered activity for THW (mGy/MBq)	0.66	0.33	0.20	0.23	0.14
THW/rhTSH ratio	6.0	1.2	1.8	2.1	1.6
3					
Absorbed dose per unit administered activity for rhTSH (mGy/MBq)	0.44	0.46	0.40	0.44	0.33
Absorbed dose per unit administered activity for THW (mGy/MBq)	0.25	0.28	0.24	0.32	0.22
THW/rhTSH ratio	0.57	0.61	0.60	0.73	0.67
4					
Absorbed dose per unit administered activity for rhTSH (mGy/MBq)	0.10	0.11	NA	NA	0.068
Absorbed dose per unit administered activity for THW (mGy/MBq)	0.11	0.10	NA	NA	0.080
THW/rhTSH ratio	1.1	0.91	NA	NA	1.2

NA = not applicable.

TABLE 4
Calculated Tumor Absorbed Dose per Unit Administered Activity of ^{131}I and Ratio in Tumor-Absorbed Dose (THW/rhTSH)

Tumor no.	Tumor volume (cm^3)	Absorbed dose per unit administered activity (mGy/MBq) for rhTSH	Absorbed dose per unit administered activity (mGy/MBq) for THW	THW/rhTSH ratio
Patient 1				
1	1.5	2.8	8.6	3.1
2	0.98	11	18	1.6
3	0.46	3.8	20	5.3
4	0.87	2.6	18	7.0
5	0.50	17	82	4.9
6	1.2	9.7	27	2.7
7	1.1	21	40	1.9
8	1.7	0.84	4.6	5.5
9	0.89	3.8	12	3.3
Patient 2				
1	0.67	0.045	1.3	28
2	0.38	0.089	2.2	25
Patient 3				
1	2.2	5.2	20	3.9
2	11	0.66	1.1	1.7
3	2.9	0.36	0.56	1.5
4	3.8	1.9	1.6	0.83
5	34	4.8	4.8	1.0
6	12	5.4	0.92	0.17
7	1.5	19	21	1.1
8	1.7	0.34	0.42	1.2
9	4.3	0.20	0.12	0.63
10	47	1.9	2.1	1.1
11	9.0	0.36	0.65	1.8

each tumor, patient, and study (rhTSH and THW) and the ratio in absorbed dose to tumors THW/rhTSH. The average absorbed dose to tumors per unit administered activity of ^{131}I was 8.0, 0.067, and 3.7 mGy/MBq for rhTSH and 26, 1.7, and 4.8 mGy/MBq for THW, for patient 1, patient 2, and patient 3, respectively. The cross-dose component from ^{131}I photons to the tumor absorbed dose of patient 1, patient 2 and patient 3 was 0.026, 0.020, and 0.075 mGy/MBq for rhTSH and 0.028, 0.037, and 0.051 mGy/MBq for THW, less than 1% compared with the tumor self-dose.

The therapeutic index, that is, the ratio of the mean tumor to bone marrow absorbed dose per unit administered activity, was 62, 0.78, and 11 for rhTSH and 232, 12, and 22 for THW, for patient 1, patient 2, and patient 3, respectively. Thus, the therapeutic index was higher in all 3 patients with lesions for THW by factors of 3.7, 16, and 2.0, respectively. Aggregate (all tumors per specific patient) tumor activity concentration was calculated for ^{124}I and plotted as a function of time for each study, rhTSH and THW, along with the calculated bone marrow activity concentration for each patient (patient 1, patient 2 and patient 3; shown in Figs. 5A, 5B, and 5C, respectively). For patients 1–3, initial activity uptake was higher in the tumors than the bone marrow.

DISCUSSION

We compared the absorbed dose to critical organs and tumors per MBq of ^{131}I administered for the treatment of distant metastases secondary to DTC by performing ^{124}I PET/CT–based dosimetry after the same patient was prepared by THW and rhTSH injections.

The 4 major distinctive features of this study are the use of ^{124}I PET/CT, the use of the 3D-RD dosimetry software, the evaluation of the absorbed dose to critical organs, and the comparison of preparations of THW versus rhTSH injections in patients who were their own control.

This study has several limitations. First, only 4 patients were studied. The prospective protocol is demanding for patients, and recruiting such patients is difficult. The patient had to undergo rhTSH-aided ^{124}I PET imaging and THW-aided ^{124}I PET imaging, and then THW-aided ^{131}I dosimetry, the latter being the standard of care for determining the maximum-tolerated prescribed activity of ^{131}I that could be administered. However, the strengths of the study were that each patient was his own control, and absorbed dose to the normal organs was calculated with ^{124}I PET/CT and 3D-RD software. Second, ^{124}I PET/CT scans prepared with rhTSH injections were always performed first, before ^{124}I PET/CT scans prepared with THW. The reverse sequence was not considered acceptable because the volunteer would have had to undergo THW twice. Although it is possible that the first study affected the subsequent one, we believe this is unlikely for the following reasons. The normal organs that were studied are not known to typically have sodium iodine symporters, so the possibility of stunning such as to normal thyroid tissue is unlikely to be present in these normal nonthyroid tissues. Although stunning from ^{124}I is possible in metastatic lesions, given the low level of ^{124}I activity, stunning in metastatic lesions is unlikely. In the unlikely scenario of stunning of the metastatic lesions from ^{124}I administration, we would expect this to reduce the uptake in the metastatic lesions, thereby reducing any production of radiolabeled T3 and T4 with ^{124}I, thus enhancing clearance from the whole body, not delaying it. A potential fourth limitation of this study is that the time interval between the 2 different preparations was approximately 5–8 wk. It is possible that during this time interval the patient's situation changed. For example, the patient's metastases could have progressed. This cannot be excluded but growth of metastases is unlikely to have affected organ clearance over the 5- to 8-wk time period. Repeated thyroglobulin levels were not available and would be less reliable because thyroglobulins are not necessarily consistent between stimulation from rhTSH injections and THW. In regard to a change in iodine intake, spot urine iodine levels were performed, but they are less than ideal and may be inadequate and problematic for several reasons. As reported by Sohn et al. (*19*) and Kim et al. (*20*), spot urine iodine levels are inferior not only to the reference standard of 24-h urine iodine measurements but also to spot urine iodine/creatinine ratios. Also, patients who were prepared with rhTSH injections continued to receive thyroid hormone, and despite a patient being compliant with his low-iodine diet, the thyroid hormone has iodine content. Patients are also variable in their compliance with a low-iodine diet. One patient had a high-urine iodine level, which was during THW. That patient had no additional urine

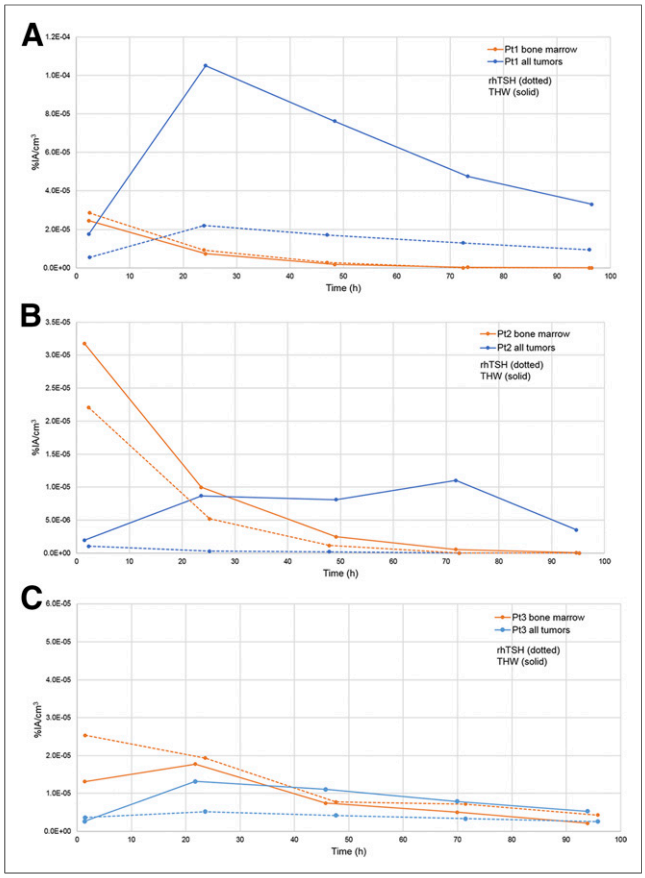

FIGURE 5. Aggregate tumor and bone marrow ^{124}I activity concentration (%IA/cm^3), rhTSH (dotted) and THW (solid) study for patient 1 (A), patient 2 (B), and patient 3 (C).

iodine level at the time of rhTSH injections. Thus, because of these factors, a limitation of the study is the inability to strictly control or adequately measure urine iodine intake. Finally, an additional limitation is possibly the low prescribed activity that was administered.

From a dosimetric standpoint, the study would have benefitted from an uncertainty analysis. However, this is a substantially complex subject and an area of active research where little in the way of definitive data or methodologies exist. Several generalities concerning uncertainties can intuitively be given: many of the systematic uncertainties will cancel out for direct comparison, the uncertainties are certainly greater for tumors than for normal organs, the combination of uncertainty and variability reinforces the notion that within this dataset neither preparation approach gives higher or lower uptake or absorbed dose for the normal organs, and that THW has a qualitatively higher therapeutic index is unlikely to be affected by any uncertainties.

Unlike the previous studies, our study evaluated multiple critical organs in patients prepared with both THW and rhTSH injections that heretofore were not all evaluated with ^{124}I and 3D-RD software. Multiple previous reports demonstrated reduced absorbed dose to the blood (e.g., bone marrow) in patients prepared with rhTSH injections (*3*–*8*). The reduced absorbed dose to the organs is attributed to the more rapid clearance of radioiodine when the patient is euthyroid versus hypothyroid (*21*). In our study, which consisted of 4 patients with metastatic disease, we observed a high patient variability in the uptake and absorbed dose results to normal organs overall between rhTSH and THW.

The absorbed dose to blood was found to be lower after stimulation with rhTSH than that in patients after THW in previous studies (*22,23*). De Keizer et al. (*23*) reported a mean absorbed dose per unit administered activity of ^{131}I to the red marrow of 0.16 ± 0.07 mGy/MBq after rhTSH-aided administration of high activities of ^{131}I. The corresponding total red marrow absorbed dose was 1.2 ± 0.52 Gy, a value lower than 2 Gy, which is the level considered the safety threshold of radioiodine therapies. The specific absorbed dose to the blood was significantly lower after administration of rhTSH (0.11 ± 0.028 mGy/MBq) than after THW (0.17 ± 0.061 mGy/MBq), in the study published by Hänscheid et al. (*8*). Luster et al. (*7*) compared the ^{131}I kinetics in patients while euthyroid and while hypothyroid and reported major differences in the residence times and absorbed doses to the blood: 0.0011 ± 2.9E−4 mGy/MBq for euthyroid versus 0.0013 ± 2.7E−4 mGy/MBq for hypothyroid patients. The mean absorbed dose per unit administered activity to the bone marrow in our study was 0.15 ± 0.12 mGy/MBq for rhTSH-aided and 0.14 ± 0.060 mGy/MBq for THW-aided administration, values comparable to the absorbed dose per unit administered activity to the bone marrow reported by de Keizer et al. (*23*) and the doses to the blood calculated by Hänscheid et al. (*8*) and higher than the doses to the blood reported by Luster et al. (*7*). However, the methods of dose calculation are different. In this study, we calculated the absorbed dose to the bone marrow of ^{131}I using the patient-specific 3D-RD software package, based on the 3-dimensional ^{124}I PET/CT imaging and VOIs covering the bone marrow region of the thoracic and lumbar vertebrae (between T9 and L4, depending on the patient). In the other studies by de Keizer et al. (*23*), Hänscheid et al. (*8*), and Luster et al. (*7*) the absorbed dose to the bone marrow is calculated on the basis of collected blood time–activity data and following the blood dosimetry method described by Sgouros et al. (*24,25*). Woliner-van der Weg et al. (*16*) compared the blood-based, planar image–based, and 3D image–based red bone marrow dosimetry (using the 3D-RD software) approaches, in terms of the absorbed dose to the red bone marrow and the predictability of red bone marrow toxicity. In this study, the authors showed that the 3D-RD–based red bone marrow dosimetry was a more sensitive predictor for the selection of patients showing any grade of red bone marrow toxicity than blood-based and planar image–based red bone marrow doses (*16*). Nevertheless, there is room for improvement in the calculation of the blood dose: a microscale model with marrow cavities, adipose cells, and trabecular bone integrated into the macroscale imaging would certainly be beneficial. The interior vertebral VOI consists of a mixture of trabecular bone and marrow space contents, that is, red and yellow marrow, blood vessels, extracellular fluid, and vasculature. In this study, it was assumed that the activity concentration within the VOI was uniform and no further corrections were applied to account for differences in activity concentration or density within the VOI. Previous studies by Schwartz et al. (*26*) and Makris et al. (*27*) have applied a correction to the red marrow activity concentration for the trabecular bone component, assuming that the activity concentration in the trabecular bone was zero. This assumption is reasonable when there is no specific binding to bone components, which is true for the radiolabeled antibodies used in these 2 studies (*26,27*). Another study by Shah et al. (*28*) provided a detailed modeling of the 3-dimensional small-scale structure of individual marrow-containing bones within the skeleton and presented estimates of absorbed fractions and S values for a variety of β-emitters. However, to our knowledge, presently

there are no methods that can accurately estimate the activity concentration in the different bone marrow regions, which is indispensable for the absorbed dose calculation. The development of such a method, combined with model-based estimates on the radionuclide S values for the bone marrow regions, would allow calculation of the absorbed dose to the different bone marrow regions, permitting improved estimates of the bone marrow absorbed dose. The latter may allow an increase in the administered activity and tumor dose, thus possibly an optimal therapeutic administration.

We found that the absorbed dose for potential ^{131}I therapy to 19 of 22 lesions was higher in the THW study than in the rhTSH study. Explanations for this have included longer stimulation by TSH that occurs with THW and slower clearance of radioiodine during hypothyroidism secondary to THW, which in turn may result in a higher bioavailability of radioiodine (*29*). The results reported here are consistent with the study conducted by Freudenberg et al. (*1*) and Potzi et al. (*3*), which reported a lower cumulated activity or lower absorbed dose to DTC metastases after rhTSH than after THW. In another study, Van Nostrand et al. (*30*) found that significantly more foci of metastases of DTC were identified in ^{124}I PET scans obtained after THW than in scans obtained after rhTSH. However, this study did not assess whether or not the detection of significantly more foci of metastases helps predict better outcomes. In addition, Klubo-Gwiezdzinska et al. (*31*) were unable to demonstrate any difference in outcomes of patients treated with ^{131}I when prepared with THW versus rhTSH.

The tumor to bone marrow absorbed dose ratio (the therapeutic index) was found to be significantly higher after THW than after rhTSH.

CONCLUSION

This study calculated the absorbed doses to normal organs including not only bone marrow, but also lung, heart, liver, and kidney as well as tumors, per MBq of ^{131}I administered in patients with metastatic differentiated thyroid cancer.

The dosimetry calculations for the normal organs were performed on the basis of the ^{124}I PET/CT imaging and using the patient-specific 3D-RD software. In addition, the patient was his own control in the comparisons between rhTSH and THW. The results suggest a high patient variability in the overall absorbed dose to the normal organs per MBq of ^{131}I administered between the 2 methods of stimulating TSH. The tumor absorbed dose per unit administered activity was higher in the THW study than in the rhTSH study for most of the tumors (~86%). The therapeutic index or the tumor–to–dose-limiting organ (bone marrow) absorbed dose ratio was higher when the patient was prepared using THW than when rhTSH was used.

Although participation in this study or similar studies is demanding for patient volunteers, further recruitment of volunteers, in particular female volunteers for this or similar studies, is warranted. In addition, studies are warranted not only to prospectively evaluate patient outcomes after ^{131}I therapy in patients prepared with rhTSH versus THW, but also to evaluate the potential benefit of THW combined with rhTSH.

In regard to the present use of rhTSH preparation in patients with metastatic DTC, we submit that until further data are available, the use of rhTSH preparation in patients who cannot tolerate THW is a reasonable alternative, and in those patients who are able to tolerate THW, we recommend that the potential benefits and risks of each preparation be explained to the patient so that each patient can make an informed decision regarding the approach taken.

DISCLOSURE

We thank our patients at MedStar Washington Hospital Center for their support. This work was also supported by NIH NCI grant R01 CA116477. No other potential conflict of interest relevant to this article was reported.

REFERENCES

1. Freudenberg LS, Jentzen W, Petrich T, et al. Lesion dose in differentiated thyroid carcinoma metastases after rhTSH or thyroid hormone withdrawal: ^{124}I PET/CT dosimetric comparisons. *Eur J Nucl Med Mol Imaging.* 2010; 37:2267–2276.
2. Taïeb D, Jacob T, Zotian E, Mundler O. Lack of efficacy of recombinant human thyrotropin versus thyroid hormone withdrawal for radioiodine therapy imaging in a patient with differentiated thyroid carcinoma lung metastases. *Thyroid.* 2004;14:465–467.
3. Pötzi C, Moameni A, Karanikas G, et al. Comparison of iodine uptake in tumour and nontumour tissue under thyroid hormone deprivation and with recombinant human thyrotropin in thyroid cancer patients. *Clin Endocrinol (Oxf).* 2006;65:519–523.
4. Rani D, Kaisar S, Awasare S. Kamaldeep, Abhyankar A, Basu S. Examining recombinant human TSH primed ^{131}I therapy protocol in patients with metastatic differentiated thyroid carcinoma: comparison with the traditional thyroid hormone withdrawal protocol. *Eur J Nucl Med Mol Imaging.* 2014;41:1767–1780.
5. Pacini F, Ladenson PW, Schlumberger M, et al. Radioiodine ablation of thyroid remnants after preparation with recombinant human thyrotropin in differentiated thyroid carcinoma: results of an international, randomized, controlled study. *J Clin Endocrinol Metab.* 2006;91:926–932.
6. Menzel C, Kranert WT, Dobert N, et al. RhTSH stimulation before radioiodine therapy in thyroid cancer reduces the effective half-life of I-131. *J Nucl Med.* 2003;44:1065–1068.
7. Luster M, Sherman SI, Skarulis MC, et al. Comparison of radioiodine biokinetics following the administration of recombinant human thyroid stimulating hormone and after thyroid hormone withdrawal in thyroid carcinoma. *Eur J Nucl Med Mol Imaging.* 2003;30:1371–1377.
8. Hänscheid H, Lassmann M, Luster M, et al. Iodine biokinetics and dosimetry in radioiodine therapy of thyroid cancer: procedures and results of a prospective international controlled study of ablation after rhTSH or hormone withdrawal. *J Nucl Med.* 2006;47:648–654.
9. Sgouros G, Frey E, Wahl R, He B, Prideaux A, Hobbs R. Three-dimensional imaging-based radiobiological dosimetry. *Semin Nucl Med.* 2008;38:321–334.
10. Prideaux AR, Song H, Hobbs RF, et al. Three-dimensional radiobiologic dosimetry: application of radiobiologic modeling to patient-specific 3-dimensional imaging-based internal dosimetry. *J Nucl Med.* 2007;48:1008–1016.
11. Sgouros G, Hobbs RF, Atkins FB, Van Nostrand D, Ladenson PW, Wahl RL. Three-dimensional radiobiological dosimetry (3D-RD) with ^{124}I PET for ^{131}I therapy of thyroid cancer. *Eur J Nucl Med Mol Imaging.* 2011;38(suppl 1): S41–S47.
12. Senthamizhchelvan S, Hobbs R, Baechler S, et al. Patient specific 3-D radiobiological dosimetry (3D-RD) for ^{153}Sm-EDTMP therapy of osteosarcoma. *SNM.* Toronto, Canada; 2009.
13. Van Nostrand D, Bandaru V, Chennupati S, et al. Radiopharmacokinetics of radioiodine in the parotid glands after the administration of lemon juice. *Thyroid.* 2010;20:1113–1119.
14. Hobbs RF, Wahl RL, Lodge MA, et al. ^{124}I PET-based 3D-RD dosimetry for a pediatric thyroid cancer patient: real-time treatment planning and methodologic comparison. *J Nucl Med.* 2009;50:1844–1847.
15. Eckerman KF, Enzo A. *MIRD: Radionuclide Data and Decay Schemes.* 2nd ed. Reston, VA: Society of Nuclear Medicine; 2008.
16. Woliner-van der Weg W, Schoffelen R, Hobbs RF, et al. Tumor and red bone marrow dosimetry: comparison of methods for prospective treatment planning in pretargeted radioimmunotherapy. *EJNMMI Phys.* 2015;2:5.
17. Bolch WE, Eckerman KF, Sgouros G, Thomas SR. MIRD pamphlet no. 21: a generalized schema for radiopharmaceutical dosimetry–standardization of nomenclature. *J Nucl Med.* 2009;50:477–484.

18. Stabin MG, Sparks RB, Crowe E. OLINDA/EXM: the second-generation personal computer software for internal dose assessment in nuclear medicine. *J Nucl Med.* 2005;46:1023–1027.
19. Sohn SY, Choi JY, Jang HW, et al. Association between excessive urinary iodine excretion and failure of radioactive iodine thyroid ablation in patients with papillary thyroid cancer. *Thyroid.* 2013;23:741–747.
20. Kim HK, Lee SY, Lee JI, et al. Usefulness of iodine/creatinine ratio from spot-urine samples to evaluate the effectiveness of low-iodine diet preparation for radioiodine therapy. *Clin Endocrinol (Oxf).* 2010;73:114–118.
21. Ladenson PW, Braverman LE, Mazzaferri EL, et al. Comparison of administration of recombinant human thyrotropin with withdrawal of thyroid hormone for radioactive iodine scanning in patients with thyroid carcinoma. *N Engl J Med.* 1997;337:888–896.
22. Sisson JC, Shulkin BL, Lawson S. Increasing efficacy and safety of treatments of patients with well-differentiated thyroid carcinoma by measuring body retentions of ^{131}I. *J Nucl Med.* 2003;44:898–903.
23. de Keizer B, Hoekstra A, Konijnenberg MW, et al. Bone marrow dosimetry and safety of high ^{131}I activities given after recombinant human thyroid-stimulating hormone to treat metastatic differentiated thyroid cancer. *J Nucl Med.* 2004;45:1549–1554.
24. Sgouros G. Bone marrow dosimetry for radioimmunotherapy: theoretical considerations. *J Nucl Med.* 1993;34:689–694.
25. Shen S, DeNardo GL, Sgouros G, O'Donnell RT, DeNardo SJ. Practical determination of patient-specific marrow dose using radioactivity concentration in blood and body. *J Nucl Med.* 1999;40:2102–2106.
26. Schwartz J, Humm JL, Divgi CR, Larson SM, O'Donoghue JA. Bone marrow dosimetry using ^{124}I-PET. *J Nucl Med.* 2012;53:615–621.
27. Makris NE, Boellaard R, van Lingen A, et al. PET/CT-derived whole-body and bone marrow dosimetry of ^{89}Zr-cetuximab. *J Nucl Med.* 2015;56:249–254.
28. Shah AP, Bolch WE, Rajon DA, Patton PW, Jokisch DW. A paired-image radiation transport model for skeletal dosimetry. *J Nucl Med.* 2005;46:344–353.
29. Van Nostrand D, Khorjekar GR, O'Neil J, et al. Recombinant human thyroid-stimulating hormone versus thyroid hormone withdrawal in the identification of metastasis in differentiated thyroid cancer with ^{131}I planar whole-body imaging and ^{124}I PET. *J Nucl Med.* 2012;53:359–362.
30. Klubo-Gwiezdzinska J, Burman KD, Van Nostrand D, Mete M, Jonklaas J, Wartofsky L. Radioiodine treatment of metastatic thyroid cancer: relative efficacy and side effect profile after preparation by thyroid hormone withdrawal vs. recombinant human TSH. *Thyroid.* 2012;22: 310–317.